Multipactor Experiments on an S-Band Coaxial Test Cell

Stephen V. Langellotti, Nicholas M. Jordan, Y. Y. Lau and Ronald M. Gilgenbach
Plasma, Pulsed Power and Microwave Laboratory
Nuclear Engineering and Radiological Sciences Department
University of Michigan
Ann Arbor, MI USA 48109-02104
The author to whom correspondence may be addressed: svlangel@umich.edu

ABSTRACT

Radiofrequency vacuum electronics are prone to multipactor discharges. These electron discharges, driven by secondary electron emission, can disrupt and damage devices and are particularly important in satellite communication systems. We present results from a new S-band coaxial multipactor test cell which demonstrates scaling to much higher frequencies (3.05 GHz) than previous coaxial experiments (10-150 MHz). The multipactor breakdown threshold has been found to agree very well with our earlier simulated predictions. The significant effect from multipactor self-conditioning has also been demonstrated and characterized. Future experiments will use this test cell to investigate various multipactor mitigation strategies.

I - INTRODUCTION

Multipactor is a discharge phenomenon that can potentially occur in vacuum electronic systems exposed to alternating electric fields[1,2]. During multipactor, RF electric fields accelerate free electrons into surfaces. When the electrons strike surfaces, secondary electron emission can occur and enable the discharge to grow. The resultant discharge can have a number of serious negative effects including cavity loading[1,2], degradation of signal quality[3], and even localized heating and catastrophic failure of the device[4]. Multipactor is particularly concerning in satellite communication systems where component repair is impossible and signal degradation can sever earthbound communications.

Preventing multipactor is essential for ensuring reliable, long term operation of RF vacuum electronic systems. In the simplest geometries (two-surface, parallel plate multipactor), analytic models can be used to generate rudimentary predictions of when multipactor will occur[1,2].

The classical theory for multipactor relies on implementing a resonance condition between the electron motion and the electric fields; in a parallel-plate geometry, electrons must impact the opposite electrode after an odd number of half-cycles. Solving the electrons' equation of motion allows one to determine the RF-voltage, electrode gap spacing, and frequency necessary to sustain a multipactor discharge[1,2]. This simple theoretical approach can be used to approximate a planar device's susceptibility to undergo multipactor[5]. Similar analytical approaches can be used to describe single-surface multipactor on planar dielectric surfaces[1].

While the classical theory for multipactor can produce reasonable predictions for planar systems, the theory becomes very difficult to implement for more complex geometries, particularly in coaxial transmission lines. In coaxial systems, the equation of motion does not have a simple analytic solution, so the classical theory must be solved numerically. Additionally, the electron trajectories from the inner to the outer conductors and vice versa are asymmetric, thus preventing any simple definition for the resonance condition. If one also considers the electrons' angular momentum, one also finds that some particles will miss the inner conductor entirely; entire single-surface modes can exist concurrently with the dominant two-surface multipactor discharge. The combination of all of these factors reveals that coaxial multipactor is extremely difficult to represent theoretically, and most analytic models are approximate by nature[6,7]. While newer theories have been developed to better describe coaxial multipactor, such as Siddiqi and Kishek's chaos model[8], they are extremely computationally expensive and their implementation is far from trivial.

Since coaxial multipactor is difficult to represent theoretically, most previous research has focused on simulated[9,10] and experimental[11,12] studies. The goal of this research is to develop a new S-band coaxial multipactor test cell for validating new theoretical models and testing advanced technologies for mitigating multipactor discharges. Previous coaxial experiments have generally focused on lower frequency ranges (10-150 MHz)[11,12] with few experiments at the GHz range[13]. The new S-band (3.05 GHz) test cell reported here supports experiments at frequencies more representative of modern high-bandwidth telecommunication devices. This work is part of a multi-university research initiative to develop multipactor test cells for several geometries, including planar[14], microstripline[15], and coaxial transmission lines[10]. We previously reported on a series of simulations to support the design of this test cell[10]. We now expand on this work to present the demonstration of our experimental test cell and experimental data characterizing its operation.

We will compare the breakdown threshold of this experimental test cell to our earlier predictions. Our experiments also have exhibited a strong effect from multipactor "self-conditioning". During this process, the multipactor electrons "clean" the electrode surfaces, removing impurities and effectively suppressing multipactor over a wider range. While this phenomenon has been acknowledged for several decades[12,16], few published studies have systematically characterized it[17]. We will present a method for controlling the self-conditioning process to ensure consistent surface conditions and repeatable multipactor discharges.

II - Experimental Design and Diagnostics

This multipactor test cell design, based on our previously reported simulations[10], consists of a coaxial transmission line suspended in a vacuum chamber, as depicted in **Fig. 1**. Two Myat 101-059 feedthrough adapters on either side of the vacuum chamber (shown in **Fig. 1a**) adapt external N-type connections to the internal transmission line. The transmission line uses a stepped coaxial design with the multipacting region (highlighted in **Fig. 1b**) at its center. The relatively small gap between the inner (highlighted in yellow) and outer conductors ensures the breakdown threshold is lowest in this region and concentrates the multipactor. At the input and output of the internal transmission line are two 50-Ω characteristic impedance segments that connect to the N-type feedthrough adapters. Two, stepped-radius, quarter-wave transformers provide an impedance match between the 50-Ω segments and the multipacting region. The outer conductor has a constant radius of 9.53 mm. The inner conductor is interchangeable and sized such that the gap between the coaxial conductors in the multipacting region is adjustable from 1.59 mm to 2.50 mm. Microwave power is supplied by an external 3.05-GHz, 40-kW magnetron with 2.5-μs pulselengths. Input power is controlled using a variable attenuator that is remotely adjustable using an Arduino-controlled stepper motor. The complete experimental test cell is shown in **Fig 1c.**

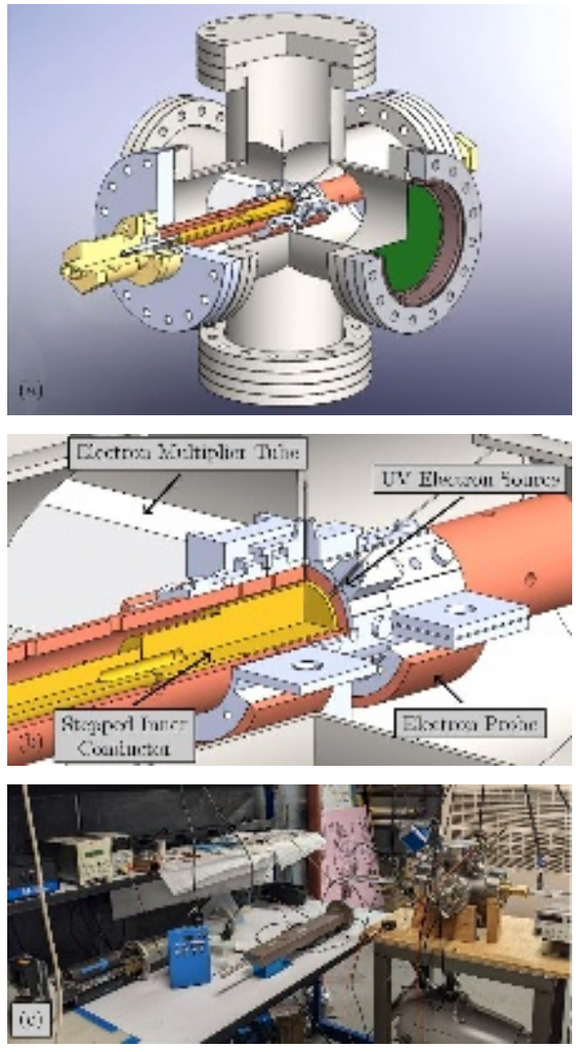

Fig. 1. (a) Experimental structure and vacuum chamber, (b) zoom in to show the layout of the diagnostics and stepped inner conductor design, and (c) complete test cell including external microwave hardware.

Figure 1b shows several diagnostics placed around the multipacting region. A series of 1-mm diameter channels in the outer conductor allow these diagnostics to access the multipactor region. Electron diagnostics include an electron multiplier tube (EMT) and two electron probes. These two sets of diagnostics allow for direct detection of the multipactor electrons. The EMT was commercially manufactured by ETP (model AF566) and directly amplifies the incoming electron current and generates an output pulse proportional to the multipactor discharge electron density. The two electron probes were developed at UM and primarily serve as binary indicators of multipactor. The design and behavior of these probes are discussed in more detail below. Also shown in **Fig. 1b** are connection points for optical fibers placed around the multipacting region.

These fibers are connected to an external 400-μW, 265-nm ultraviolet (UV) LED. Assuming a quantum efficiency[18] on the order of 10^{-3}, and the UV photons are transmitted to the copper surfaces with perfect efficiency, then the seed electron current is estimated at approximately $I_e \approx 85$ nA. The UV photons cause the copper surfaces to emit electrons, which seed the multipactor discharges. The seed electrons reduce the time between the start of the RF-pulses and the onset of multipactor. When the experiment is operated near the multipactor threshold, the electron phase-space that supports multipactor discharges is very small[1,2]. Due to the low RF duty cycle, many pulses may occur before any seed electrons that satisfy this phase-space condition appear. The UV diode increases the background electron density, increasing the population of favorable seed electrons and ultimately reducing the time before multipactor is observed. For the experiments presented in this paper, the strength and presence of the UV seeding source did not appear to affect the multipactor breakdown threshold or other multipactor behavior beyond reducing this waiting time.

Three RF diode detectors are connected to directional couplers at the input and output of the chamber and provide measurements of forward, reflected, and transmitted power in the multipactor transmission line. During our experiments, we have found that these power measurements are the most reliable indicators of multipactor discharges. Examples of the forward, reflected and transmitted power signals for a multipacting discharge are shown in **Fig. 2**. After the RF pulse begins, there is generally a delay-time before the multipactor discharge initiates. This delay-time is affected by several factors, particularly the power level and the strength of the electron-seeding source used. After this delay-time, it is observed that the reflected and transmitted power signals decrease suddenly. This effect is particularly pronounced in the reflected power signal. At the beginning of this decrease, the multipactor discharge electron density is sufficient to absorb a measurable amount of RF power, reducing both the reflected and transmitted power signals. The multipactor discharge continues to grow and soon reaches saturation (within 50-100 ns). At this point the discharge electron density is no longer growing and the power signals reach steady-state.

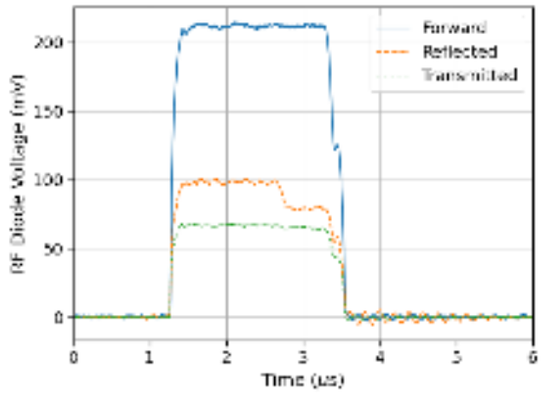

Fig. 2. Forward, reflected, and transmitted power signals during a multipacting discharge.

A cutaway view of the electron probes is shown in **Fig 3**. The electron probes are devices for detecting the presence of a multipactor discharge. They consist of a 3D-printed support structure and a copper collector plate. Multipactor electrons pass through three of the electron channels in the outer conductor and collide with the collector plate. We estimate the probes have a capacitance on the order of 50 nF; when the probes are terminated at 1 MΩ, then $RC \approx 50\ \mu$s, which is much longer than the RF pulse duration. During multipactor, when the colliding electrons charge the collector plate-capacitance, the probes thus produce a voltage pulse measured using an oscilloscope.

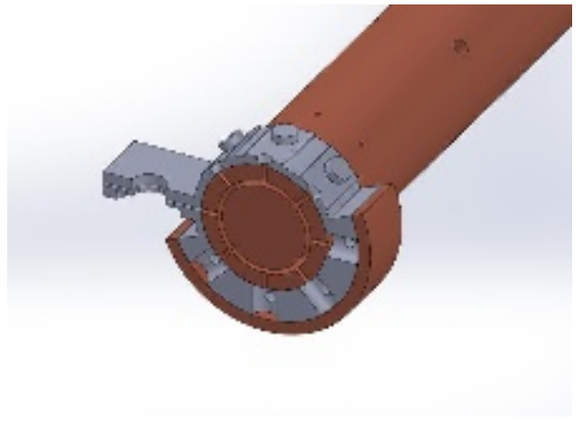

Fig. 3. Cross-section of one of the electron probes. Shown are the inner and outer conductors of the multipacting transmission lines, the 3D-printed support structure, and the copper collector plate. Not shown is the cable connecting the collector plate to the external 1-MΩ termination.

III –Multipactor Breakdown Threshold Measurements and Results

An example of the raw electron probe signal pulse is shown **Fig. 4.** Also shown for reference are the forward and reflected power signals. After the multipactor discharge initiates (as shown by the sudden drop in the reflected power signal), it quickly reaches saturation. During this steady-state period, the electron current impacting the probe's collector plate is relatively constant. Since the RC time constant is much longer than the duration of the multipactor discharge, this steady-state impact current causes the probe voltage to increase linearly. Once the RF pulse terminates and the multipactor discharge dissipates, the signal voltage reaches steady-state. This DC offset indicates whether or not multipactor has occurred. Note that the probe signal is very noisy during both the rise and fall times of the RF pulse, likely due to interference from the high voltage modulator used to drive the magnetron. A 5-MHz digital lowpass filter was applied during post-processing to remove much of this noise and to reveal the linear growth region of the signal, which agrees well with the reflected power signal. Regardless of the noise, the final DC offset is always clearly discernable and is indicative that multipactor has occurred.

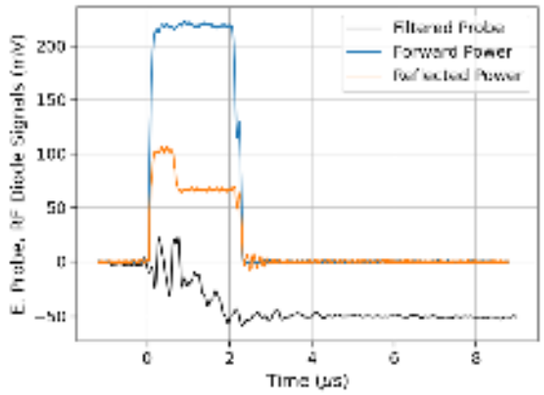

Fig. 4. Example of the filtered (black) electron probe response compared to the forward (blue) and reflected (orange) power signals.

The breakdown threshold is measured by slowly increasing the applied RF power until multipactor is observed. Voltage is applied to the driver magnetron in 2.5-μs pulses with a repetition rate of approximately 17 Hz. The external variable attenuator is slowly adjusted to increase the power level. During the process, the operator is observing power traces on the oscilloscope. The breakdown threshold is reached when the reflected power signal begins to show the characteristic dip (**Fig. 2)**. When the discharge is near the breakdown threshold, the effect on

the reflected power signal is often very subtle, so multiple measurements (typically ten) are taken to ensure repeatability and to account for variations in the operator's judgement.

Multipactor discharges are highly dependent on the surface characteristics of the transmission line electrodes. In particular, surface conditioning and outgassing due to the multipactor discharge itself have been shown to strongly affect the breakdown threshold[12,17] and have been used as a preventative measure in accelerator systems to prevent multipactor during normal operations[16]. In the present experiment, this conditioning process significantly affects the breakdown threshold. In particular, when the transmission line electrodes are "fresh", or recently exposed to air, the breakdown threshold is extremely variable and cannot be measured consistently.

Before measuring the breakdown threshold, the electrode surfaces are conditioned with high power (typically 9-10 kW) multipactor discharges for periods of fifteen minutes to ensure that all measurements are comparable. Between each exposure period, the breakdown threshold is measured and plotted relative to the total conditioning time. During these exposure periods, the RF power is applied using 2.5-μs pulses with a repetition rate of approximately 17 Hz. This process is repeated until further multipactor exposure no longer significantly affects the breakdown threshold. At this point, the electrodes are considered to be fully conditioned and are ready for experimental measurements.

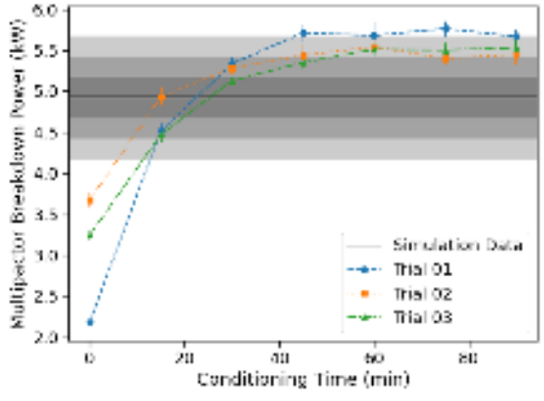

Fig. 5. Multipactor breakdown threshold as a function of conditioning time. Shaded regions represent 5, 10, and 15% agreement with CST simulations. These data are measured using $fd = 6.10$ GHz-mm.

The conditioning process is illustrated in **Fig. 5** which shows the multipactor breakdown threshold as a function of the total conditioning time. These data were measured during three testing sessions separated by a minimum of 16 hours to ensure repeatability. Error bars represent the standard deviation of ten consecutive measurements taken between each conditioning step.

Before conditioning, the breakdown threshold is highly inconsistent. However, after the first 15-minute exposure period, the three datasets begin to converge, and all three datasets reach a conditioned state after 45 minutes. The breakdown thresholds in **Fig. 5** are plotted relative to the predicted breakdown threshold from CST Particle Studio simulations[10]. Once the electrodes are fully conditioned, the breakdown threshold is consistently within 10-15% of the simulated value.

Note that this process occurs in less than 115 ms of active multipactor time. While the entire conditioning process takes 45 minutes, microwave power is only applied in 2.5-μs pulses with a repetition rate of approximately 17 Hz; (duty cycle of 4.25×10^{-5}). This is particularly noteworthy in comparison to continuous wave (CW) multipactor experiments, such as those by Woo[12] and Graves[11]. During such experiments, where the power level is controlled manually[12] or is averaged over several seconds[11], the conditioning process occurs extremely quickly and would not be readily apparent in any breakdown threshold measurements.

IV –Discussion of Results

Our previous work[10] presented a series of CST Particle Studio simulations for predicting the multipactor breakdown threshold for our experimental coaxial transmission line. We present new data here to experimentally verify these simulations. The susceptibility diagram for the experimental transmission line is shown in **Fig. 6**. Each data point represents the average breakdown threshold of ten measurements taken during a particular testing session. The breakdown threshold was measured during multiple sessions to ensure it does not drift from day-to-day.

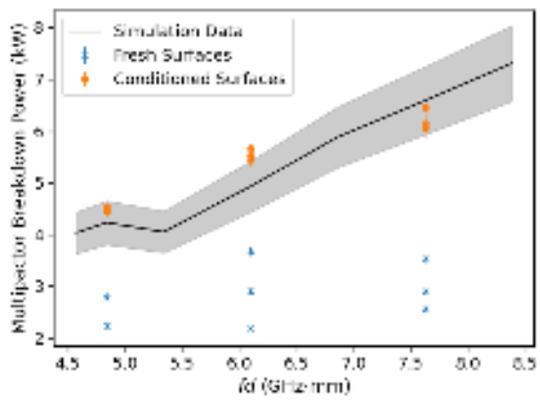

Fig. 6. Susceptibility diagram for the experimental transmission line. Experimental data are compared to simulations (black) [10]. The gray-shaded region represents agreement to within 10% of the simulated susceptibility data.

Figure 6 shows that the breakdown threshold clearly falls into two regimes, highlighting the importance of the conditioning process. When the surfaces are "fresh", the breakdown threshold is far below the simulated prediction and is highly variable. However, after conditioning the transmission line using the method described above, measured breakdown thresholds are more consistent and are within 10-15% of the simulated data.

VI - CONCLUSIONS

We have developed a coaxial test cell for studying multipactor at multi-GHz frequencies. These experiments significantly expand the scaling to much higher frequencies (3.05 GHz) than the previous coaxial multipactor research by Graves[11] (40-150 MHz) and Woo[12] (10-150 MHz). This test cell uses multiple diagnostics for detecting and measuring multipactor discharges. Comparisons between simulations and experiment show very good agreement; the observed breakdown threshold is consistently within 10-15% of the predicted values. We have also demonstrated and characterized the multipactor self-conditioning process, which greatly affects the surface characteristics of the multipacting transmission line. While surface conditioning can greatly affect the repeatability and consistency of the multipactor discharges, the process requires relatively short discharge times.

Future experiments will include testing various strategies for mitigating and preventing multipactor. Such strategies include argon plasma cleaning, surface coatings and treatments, and varying the porosity of the outer and inner conductors. Other experiments will include measuring the delay for multipactor onset and comparing our experimental data to theoretical predictions from Siddiqi and Kishek's chaos model[8].

ACKNOWLEDGEMENTS

This research was supported by AFOSR MURI #FA9550-18-1-0062 and #FA9550-21-1-0367 through Michigan State University, L3Harris Electron Devices Division, and by the Directed Energy Professional Society.

DATA AVAILABILITY

The data that support the findings of this study are available from the corresponding author upon reasonable request.

REFERENCES

[1] R.A. Kishek, Y.Y. Lau, L.K. Ang, A. Vafells, and R.M. Gilgenbach, Phys Plasmas **5**, 2120 (1998).
[2] J.R.M. Vaughan, IEEE T Electron Dev **35**, 1172 (1988).
[3] P.Y. Wong, Y.Y. Lau, P. Zhang, N. Jordan, R.M. Gilgenbach, and J. Verboncoeur, Phys Plasmas **26**, 112114 (2019).
[4] J.R.M. Vaughan, IRE T Electron Dev **8**, 302 (1961).
[5] M. Mirmozafari, N. Behdad, and J.H. Booske, Phys. Plasmas **27**, 113510 (2020).
[6] R. Udiljak, D. Anderson, M. Lisak, V.E. Semenov, and J. Puech, Phys Plasmas **14**, 033508 (2007).
[7] E. Sorolla, A. Sounas, and M. Mattes, Phys Plasmas **22**, 033512 (2015).
[8] M. Siddiqi and R. Kishek, IEEE Trans. Electron Devices **66**, 4403 (2019).
[9] V.E. Semenov, N. Zharova, R. Udijak, D. Anderson, M. Lisak, and J. Puech, Phys Plasmas **14**, 1 (2007).
[10] S.V. Langellotti, N.M. Jordan, Y.Y. Lau, and R.M. Gilgenbach, IEEE Trans. Plasma Sci. **48**, 1942 (2020).
[11] T.P. Graves, Experimental Investigation of Electron Multipactor Discharges at Very High Frequencies, PhD Thesis, Massachusetts Institute of Technology, 2006.
[12] R. Woo, J Appl Phys **39**, 1528 (1968).
[13] D. Gonzalez-Iglesias, O. Monerris, B.G. Martinez, M.E. Diaz, V.E. Boria, and P.M. Iglesias, IEEE Trans. Electron Devices **63**, 4096 (2016).
[14] Z.C. Shaw, A. Garcia, M. Powell, J.C. Dickens, J.J. Mankowski, and A.A. Neuber, Rev. Sci. Instrum. **90**, 054702 (2019).
[15] M. Mirmozafari, N. Behdad, and J.H. Booske, Rev. Sci. Instrum. **92**, 084706 (2021).
[16] A.J. Hatch, Nucl. Instrum. Methods **41**, 261 (1966).
[17] T.P. Graves, R. Spektor, P. Stout, V. Bobkov, and J.-M. Noterdaeme, in (Gent (Belgium), 2009), pp. 253–256.
[18] C.N. Berglund and W.E. Spicer, Phys. Rev. **136**, A1044 (1964).

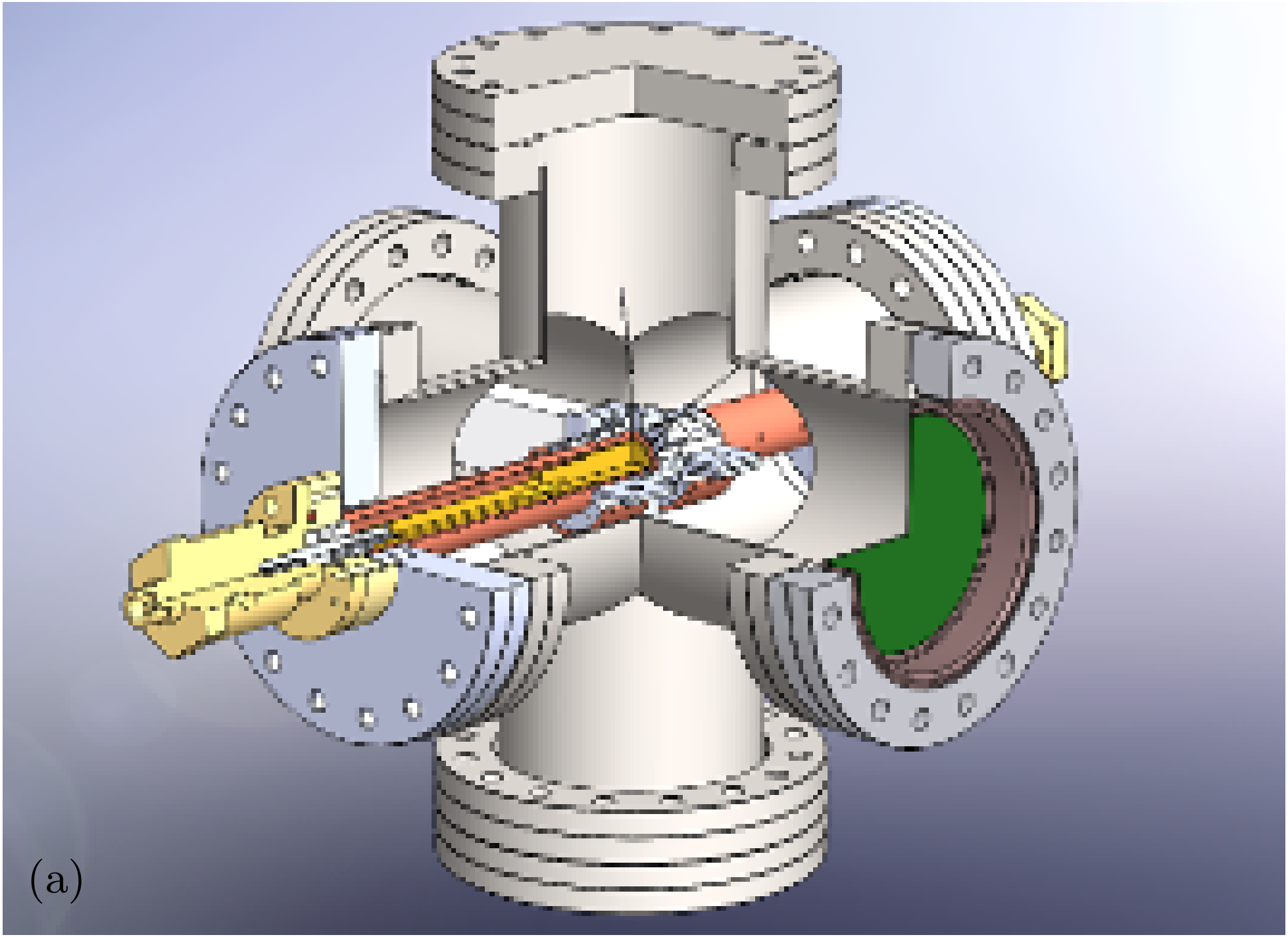

(a)

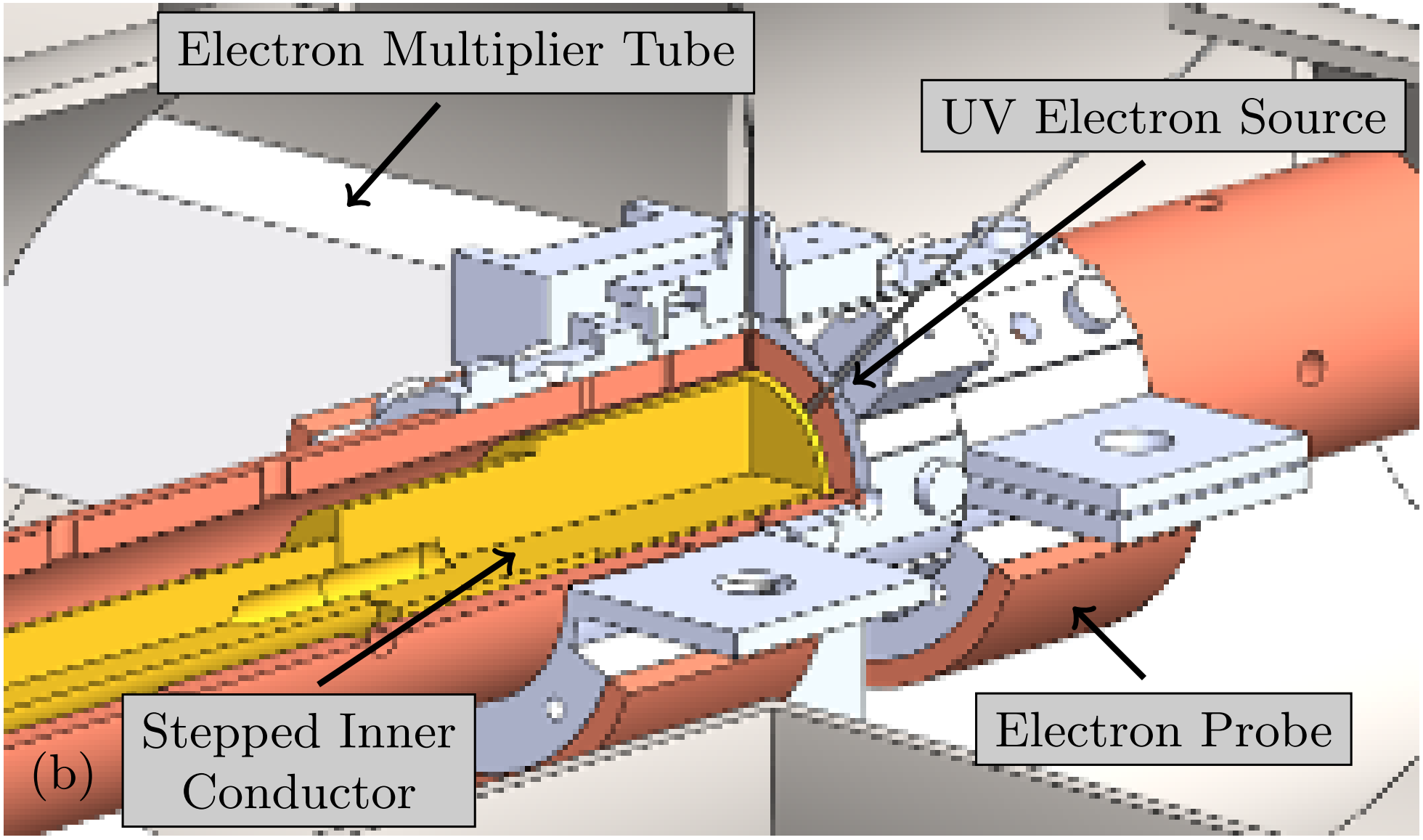
Electron Multiplier Tube
UV Electron Source
Stepped Inner Conductor
Electron Probe
(b)

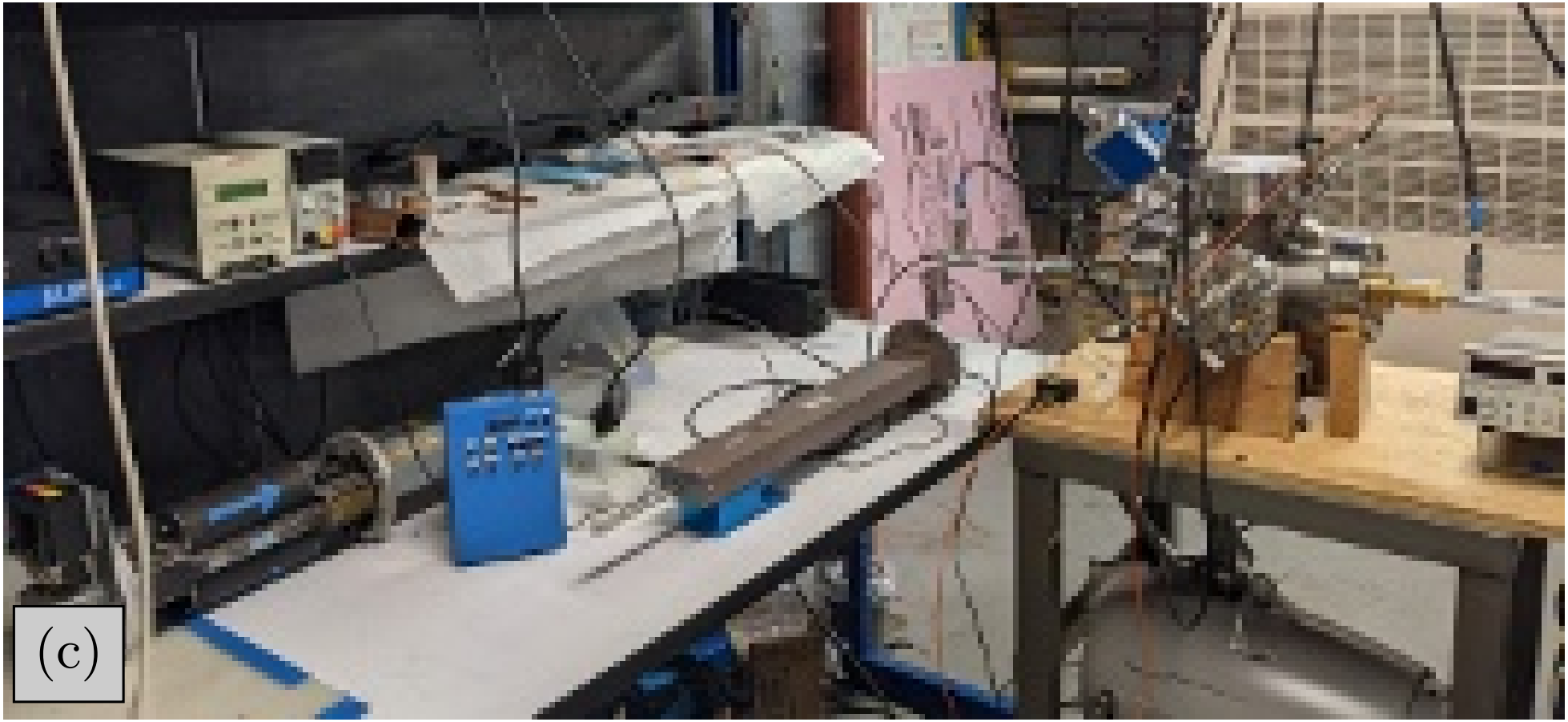
(c)

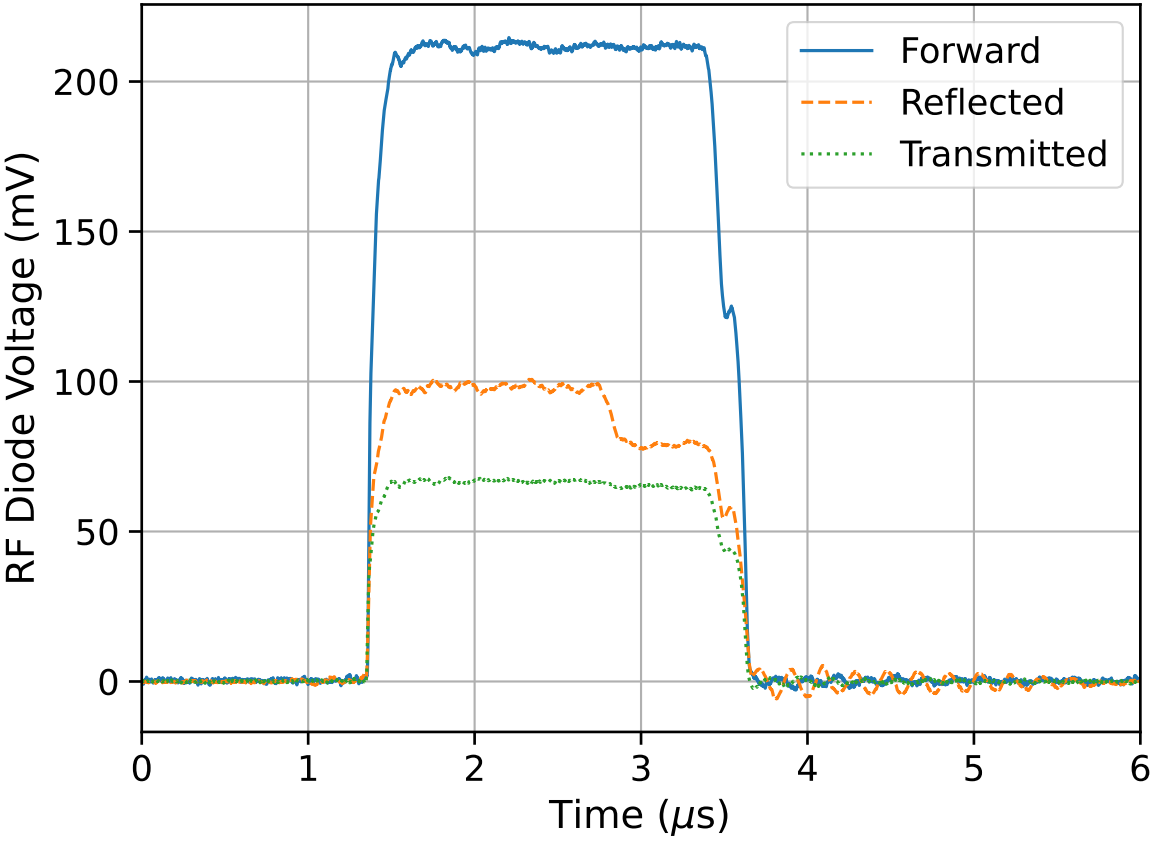
Forward
Reflected
Transmitted
RF Diode Voltage (mV)
200
150
100
50
0
0
1
2
3
4
5
6
Time (μs)

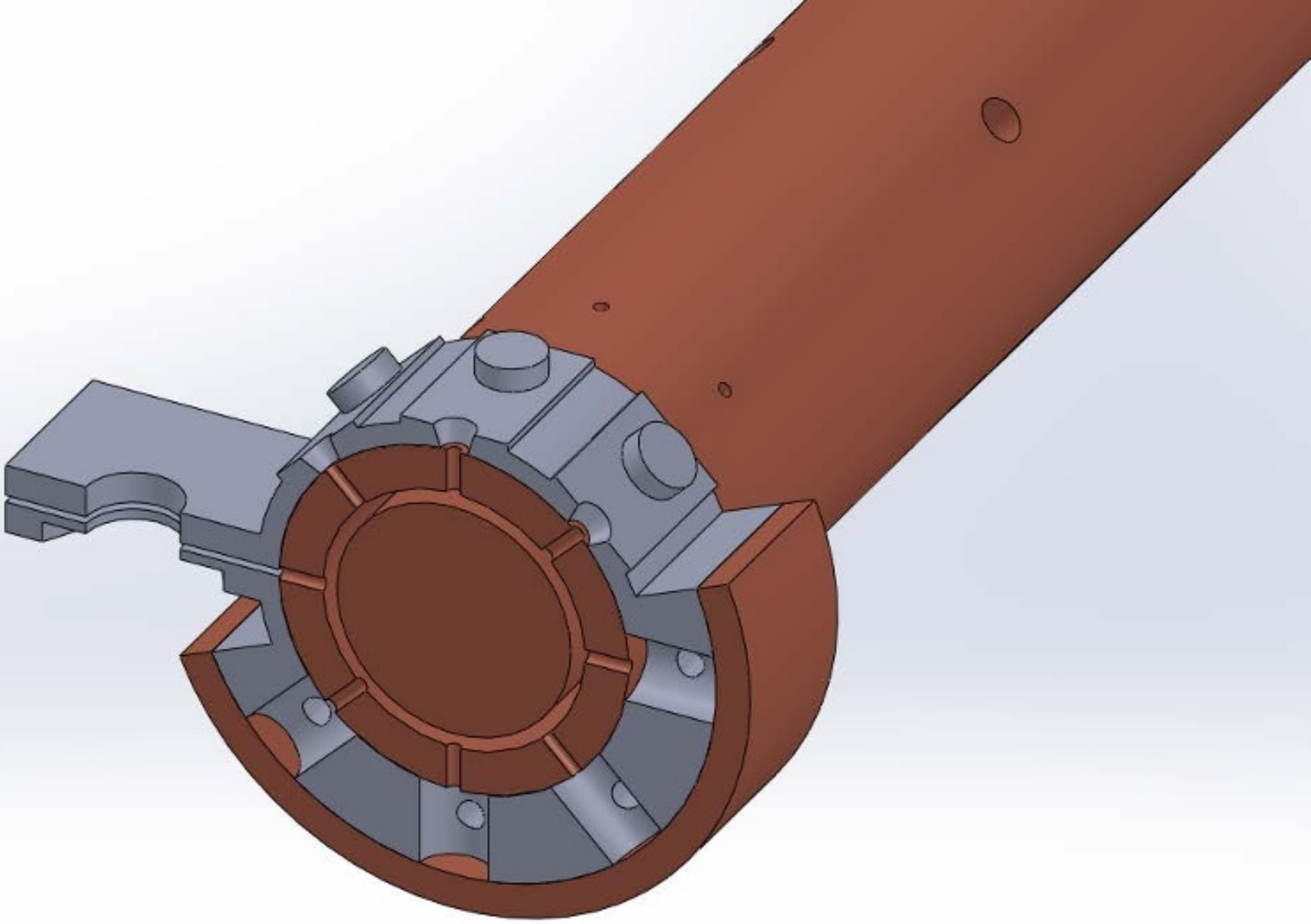

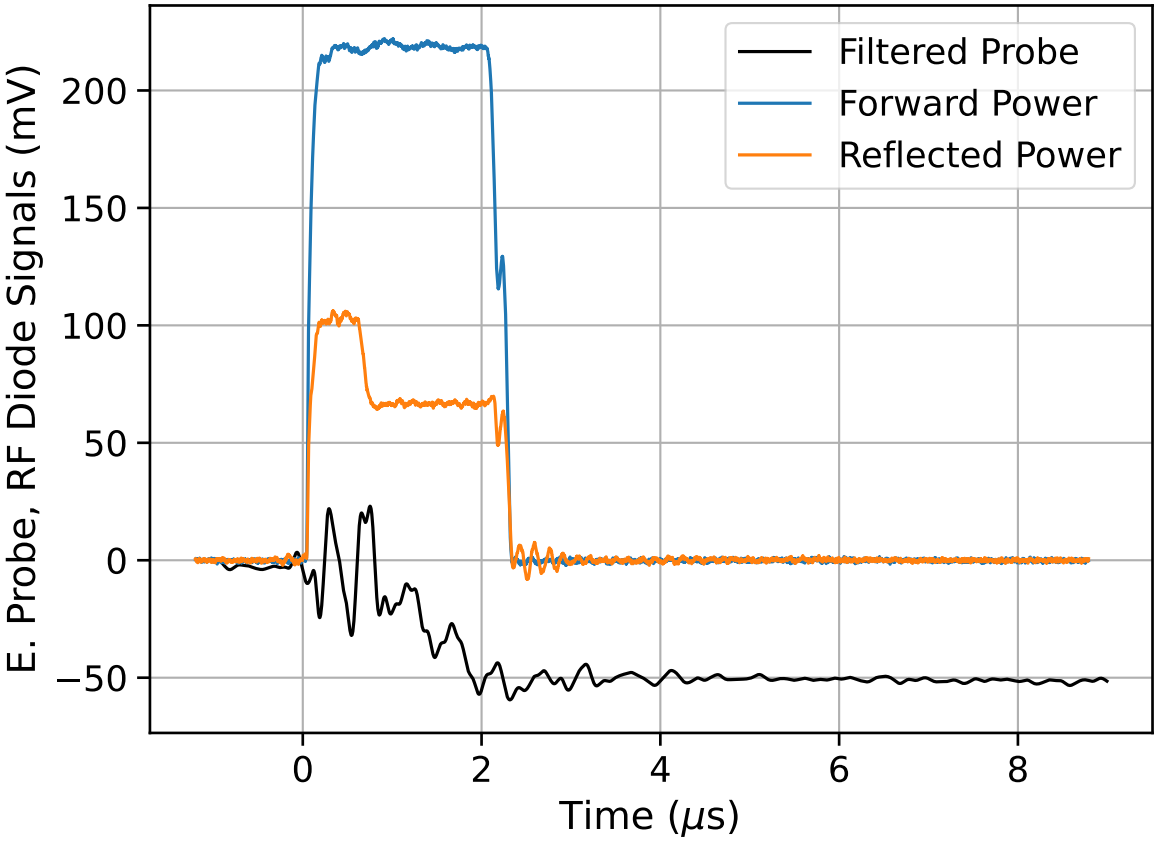
Filtered Probe
Forward Power
Reflected Power
E. Probe, RF Diode Signals (mV)
200
150
100
50
0
−50
0
2
4
6
8
Time (μs)

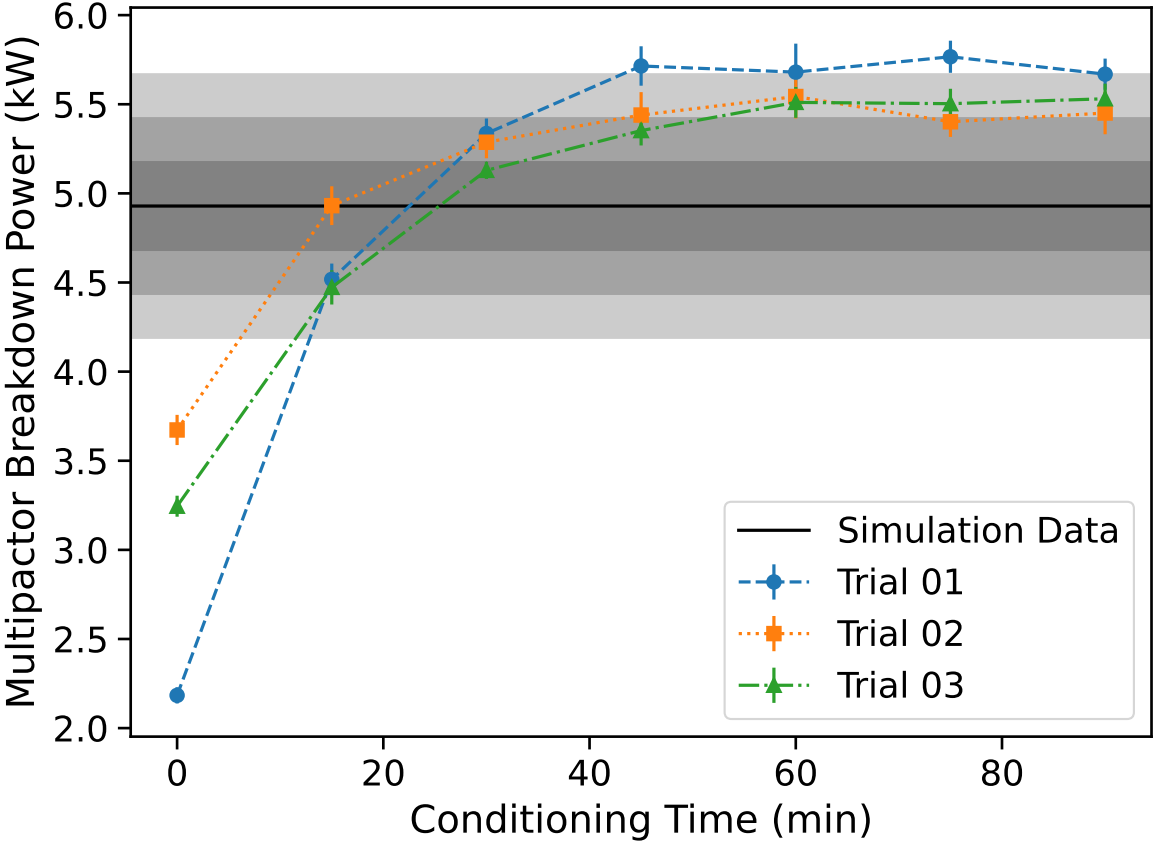
Multipactor Breakdown Power (kW)
6.0
5.5
5.0
4.5
4.0
3.5
3.0
2.5
2.0
0
20
40
60
80
Conditioning Time (min)
Simulation Data
Trial 01
Trial 02
Trial 03

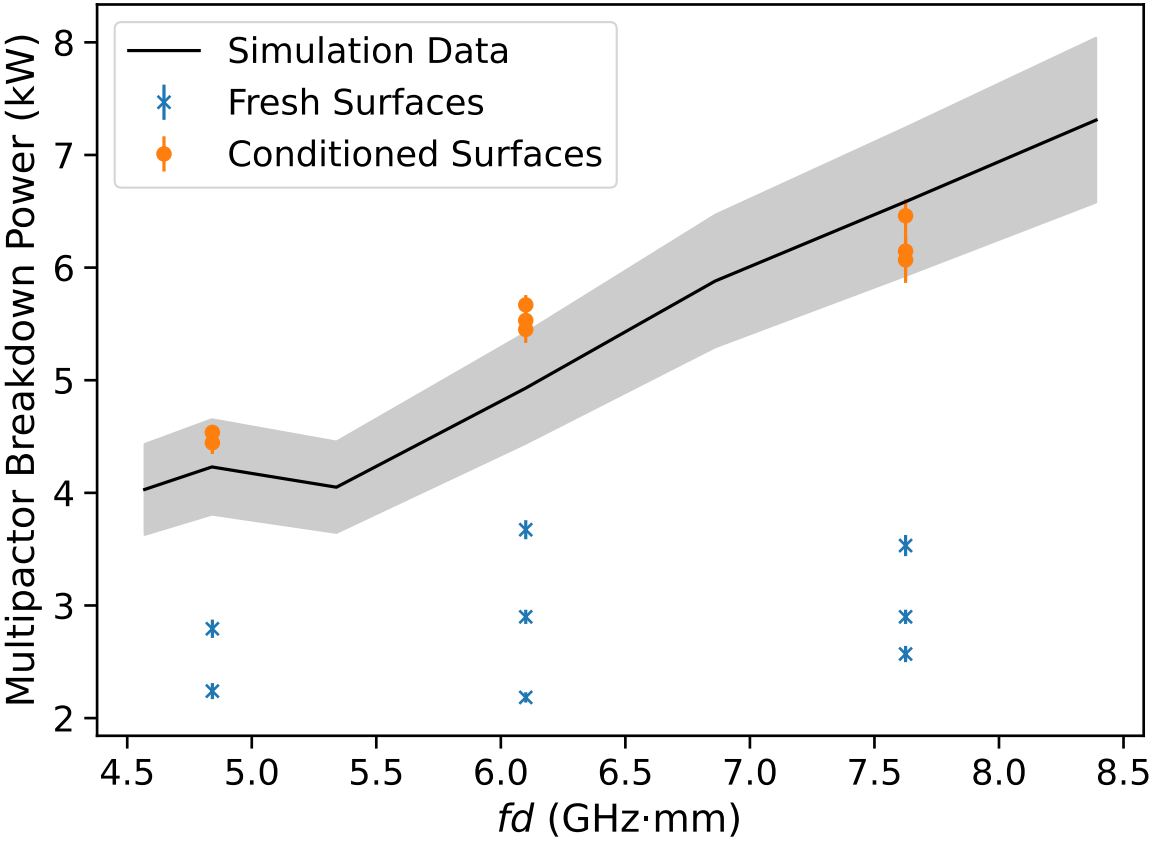
Simulation Data
Fresh Surfaces
Conditioned Surfaces
Multipactor Breakdown Power (kW)
2
3
4
5
6
7
8
4.5
5.0
5.5
6.0
6.5
7.0
7.5
8.0
8.5
fd (GHz·mm)